Letter

High-field $1/f$ noise in hBN-encapsulated graphene transistors

A. Schmitt,[1,*] D. Mele,[1,2] M. Rosticher,[1] T. Taniguchi,[3] K. Watanabe,[3] C. Maestre,[4] C. Journet,[4] V. Garnier,[5] G. Fève,[1] J. M. Berroir,[1] C. Voisin,[1] B. Plaçais,[1,†] and E. Baudin[1,‡]

[1]*Laboratoire de Physique de l'Ecole Normale Supérieure, ENS, Université PSL, CNRS, Sorbonne Université, Université Paris-Cité, 24 rue Lhomond, 75005 Paris, France*

[2]*Université Lille, CNRS, Centrale Lille, Université Polytechnique Hauts-de-France, Junia-ISEN, UMR 8520-IEMN, F-59000 Lille, France.*

[3]*Advanced Materials Laboratory, National Institute for Materials Science, Tsukuba, Ibaraki 305-0047, Japan*

[4]*Laboratoire des Multimatériaux et Interfaces, UMR CNRS 5615, Université Lyon, Université Claude Bernard Lyon 1, F-69622 Villeurbanne, France*

[5]*Université de Lyon, MATEIS, UMR CNRS 5510, INSA-Lyon, F-69621 Villeurbanne cedex, France*

(Received 13 February 2023; revised 22 March 2023; accepted 27 March 2023; published 10 April 2023)

$1/f$ electronic noise is a conductance fluctuation, expressed in terms of a mobility "α-noise" by Hooge and Kleinpenning. Understanding this noise in graphene is key for high-performance electronics. Early investigations pointed out a deviation from the standard Hooge formula, with the free-carrier density substituted by a constant density $n_\Delta \sim 10^{12}$ cm^{-2}. Here we investigate hBN-encapsulated graphene transistors where high mobility gives access to the velocity-saturation regime. We show that α-noise is still accounted for by the Hooge formula on substituting conductance by differential conductance G, resulting in a bell-shaped dependence of flicker noise with bias voltage. The same analysis holds in the Zener regime at even larger bias, with two main differences. The first one is a strong enhancement of the Hooge parameter reflecting the hundred-times larger coupling of interband excitations to the hyperbolic phonon-polariton (HPhP) modes of the midinfrared Reststrahlen (RS) bands of hBN, which is supported by microwave noise thermometry measurements. The second is an exponential suppression of this coupling at large fields, which we attribute to decoherence effects. The phenomenology of $1/f$ noise in graphene supports a quantum-coherent bremsstrahlung interpretation of α-noise.

DOI: 10.1103/PhysRevB.107.L161104

I. INTRODUCTION

Flicker ($1/f$) noise is a type of noise that dominates the spectral density at low frequencies. Ubiquitous in condensed matter and quantum conductors [1], it has also been measured in a large variety of systems ranging from biology [2] to economics [3], including nanofluidics [4]. In electronics, flicker noise is a conductance fluctuation revealed as an excess low-frequency current noise, of spectral density $S_I = CI^2/f$, superimposed on the Johnson-Nyquist thermal noise $S_{\rm th} = 4Gk_BT$ at finite bias current I. Despite almost a century of research, its origin remains controversial. In semiconductors, $1/f$ noise is usually well described using the McWorther model relying on carrier number fluctuations due to defect traps [5,6]. Alternative mechanisms based on carrier-number-fluctuations or mobility-fluctuations were proposed [7]. As pointed out by Hooge and Kleinpenning [8], the noise amplitude C is a bulk effect that can be conveniently expressed in terms of a mobility noise, called α-noise, with an intensive Hooge parameter $\alpha_H = NC$, where N is the number of carriers participating to the conductance. Measurements in both metals [9] and semiconductors [10] have yielded a quasi-universal Hooge parameter $\alpha_H \sim 2$–5×10^{-3}. A leading interpretation of the α-noise relies on a distribution of two-level fluctuators that locally and elastically modulate electronic transmission [10,11]. An alternative interpretation, based on a quantum theory proposed by Handel [12,13], points to an infrared (IR) bremsstrahlung origin which leads to a $1/f$ noise spectrum with a universal $\alpha_H = 2\alpha_0/\pi = 4.6\times10^{-3}$ in the quantum-coherent regime, where $\alpha_0 = 1/137$ is the vacuum fine-structure constant that controls light-matter coupling. This interpretation puts the emphasis on an inelastic origin of conductance noise; a critical discussion can be found in Refs. [14,15]. These contrasted interpretations take root in the ambivalent nature of conductivity, which is both a momentum relaxation coefficient $\sigma_1(t) = (J/E)(t)$ and an energy relaxation parameter in the Joule power density $\sigma_2(t) = (P/E^2)(t)$. Whereas $\sigma_1 = \sigma_2$ on average, they may differ in their time dependencies due to different scattering mechanisms and times.

Graphene is an attractive platform for flicker noise investigation because of the tunability of the charge carrier density and polarity. It also presents strong potential for electronics [16] for which flicker noise is an important performance limit [17]. Most experiments so far were carried out at low to moderate bias in diffusive low-mobility SiO_2-supported graphene transistors, with a $1/f$ corner frequency

*aurelien.schmitt@phys.ens.fr
†bernard.placais@phys.ens.fr
‡emmanuel.baudin@phys.ens.fr

in the sub-MHz range [18,19]. Flicker noise was characterized by a weakly doping-dependent flicker amplitude $A = (fS_I/I^2)LW \in [10^{-7}, 10^{-6}]$ μm^2 [16], where L and W the length and width of the graphene channel. This quasi-doping-independent value for graphene violates the Hooge empirical formula where $A = \alpha_H/n$, with n the carrier density (considering independent electrons), but points to substituting n by an unknown constant density n_Δ in a collective picture. Some reports also point to a flicker noise dip at charge neutrality [19,20], but charge neutrality corresponds to a nonlocal mesoscopic regime that deviates from standard local-transport α-noise conditions. The same occurs under intense magnetic fields, with a field-induced noise reduction [21], leading to a full suppression enforced by conductance quantization [22]. A deviation from the above $A = Cte$ diffusive graphene flicker noise was reported in moderate-mobility suspended samples, where a noise reduction was observed [23].

The high-mobility hBN-encapsulated graphene transistors investigated in the present work constitute a test bed for α-noise as we study it in an extended electric-field range with different scattering and relaxation mechanisms upon increasing bias. In the perspective of testing the bremsstrahlung interpretation, the use of hBN-encapsulates is an additional asset, as hBN not only provides a superior mobility [24], but also a very characteristic midinfrared (MIR) near-field electromagnetic environment [25,26], with its two Reststrahlen (RS) bands, $\hbar\Omega_I = 95$–100 meV and $\hbar\Omega_{II} = 170$–200 meV. Recent experiments indeed showed that the hyperbolic light of these RS bands strongly couples to graphene electronic transport [27–29]. The three electronic transport regimes observed in increasing bias are (i) the mobility-limited Drude regime at low field, (ii) the velocity saturation regime for $E \gtrsim E_{\rm sat} = v_{\rm sat}/\mu(0)$ where $v_{\rm sat}$ is the phonon-limited saturation velocity and $E_{\rm sat}$ the saturation field, and finally (iii) the interband Zener regime characterized by a doping and bias-independent differential conductivity σ_Z. Based on combined transport, flicker, and thermal noise characterization in a series of high-quality samples, we show that (i) the standard analysis of flicker noise in graphene can be consistently extended to the nonlinear saturation regime and (ii) the interband Zener contribution can be accounted for by introducing a semi-empirical formula in the spirit of the bremsstrahlung interpretation, accounting for the enhanced electromagnetic coupling of interband excitations and decoherence effects.

II. SAMPLE DESCRIPTION AND NOISE MEASUREMENTS

We use a series of ten hBN-encapsulated graphene transistors, of a large size $(L, W) = 4 - 25$ μm and low edge-contact resistance R_c, exhibiting large mobility μ= 2–15 m^2/Vs, saturation velocity $v_{\rm sat} = 0.2$–$0.8 v_F$, and Zener conductivity $\sigma_Z =$ 0.1–1 mS, as described in Supplementary Material Table-SI-1 [30]. They map a broad range of hBN dielectric thickness $t_{\rm hBN} = 50$–160 nm and a variety of gating: (IR reflecting) Au bottom-gates, (IR absorbing) graphite bottom-gates, and SiO_2-insulated Si backgates. We also use two different hBN grades: the high-pressure high-temperature (HPHT) from National Institute for Materials Sciences (NIMS) [31], and the polymer-derived ceramic (PDC) from Lyon [32,33] which behave differently. All devices are embedded in coplanar waveguides for the room-temperature probe-station measurement of DC transport, sub-MHz flicker noise, and microwave thermal noise [see Fig. 1(a)]. High-mobility transistors sustain large saturation currents (∼1 mA/μm), rejecting the $1/f$ noise corner frequency in the low GHz range and allowing a double-check of the flicker noise with the GHz noise spectra.

Current noise is analyzed with a modified Hooge formula $S_I = C(GV)^2/f$, obtained by substituting the total current I by the differential current GV to account for nonlinear transport [17]. Here V is the channel drain-source voltage, $G = \partial I/\partial V = [ne\mu(E) + \sigma_Z]W/L$ is the differential conductance where $\mu(E) = \mu(0)/(1 + E/E_{\rm sat})^2$ is the optical phonon-limited mobility. We apply the biasing procedure described in Ref. [27] to correct for drain-gating effect, ensuring quasi-homogeneous doping and electric fields and rejecting drain pinch-off effect, such as was investigated in Ref. [34]. Low-frequency noise characterization is enriched by thermal noise measurements, performed in the flicker-free [27] microwave (1–10 GHz) band. This allows estimating the electronic temperature T_N and the thermal conductivity dP/dT_N ($P = VI/LW$ is the areal Joule power) to the hBN substrate which turns on in the Zener regime [29].

Figure 1(a) shows typical current-voltage curves measured in the representative transistor "GrS5." They show the successive low-bias linear ohmic behavior, the velocity-saturation regime for $V > V_{\rm sat} \simeq 0.25$ V, and finally the interband Zener regime. The saturation of intraband current can be consistently attributed to the scattering of electrons by the optical phonons of the lower RS band of hBN [27]. The Zener regime is accompanied by the onset of energy relaxation by optical phonons of the upper RS band of hBN [27,28]. Its main signature is electron cooling that is observed in the noise temperature [inset of Fig. 3(c)] by a decrease of the temperature-field slope that can even turn to a temperature drop with bias in bilayer graphene [29].

As illustrated in Fig. SI-3, the differential conductivity is accurately fitted using the sum of saturation ($\sigma_{\rm sat}$) and Zener (σ_Z) contributions [27,35] $\sigma(E) = ne\frac{\mu(0)}{(1+E/E_{\rm sat})^2} + \sigma_Z$, where μ(0) the low-bias mobility, n the carrier density, and $E = V/L$. We disregard Zener tunneling suppression due to Pauli blocking at low field [27,29], as it involves minute corrections to the intraband conductivity and noise. From these fits we extract DC transport parameters μ(0), $E_{\rm sat}$ or $v_{\rm sat}$ and σ_Z that are listed in Table SI-1.

For each bias and doping, we measure the current noise in the $f = [0.1$–$1]$ MHz band, as shown in Fig. 1(b). Flicker noise corresponds to plateaus $fS_I(f) = a + bf$, where a is the amplitude of flicker noise and b measures the instrumental background noise. The amplitude a has an asymmetric bell-shaped bias dependence [Fig. 1(c)], and a strong doping dependence $fS_I \propto n^2$ (which is confirmed by the representation of the doping-independent velocity flicker noise $S_v = S_I/n^2e^2W^2$ in Fig. SI-5). The noise amplitude $A = fS_I/(GV)^2(WL)$ is plotted in the inset of Fig. 1(c). Its low-bias extrapolate $A \sim 10^{-7}$ μm^2 is consistent with diffusive graphene values [16]. At high bias we observe an amplitude suppression, with A following an exponential dependence $A \propto e^{-E/E_\Lambda}$, with a characteristic electric field $E_\Lambda \sim 0.1$ V/μm.

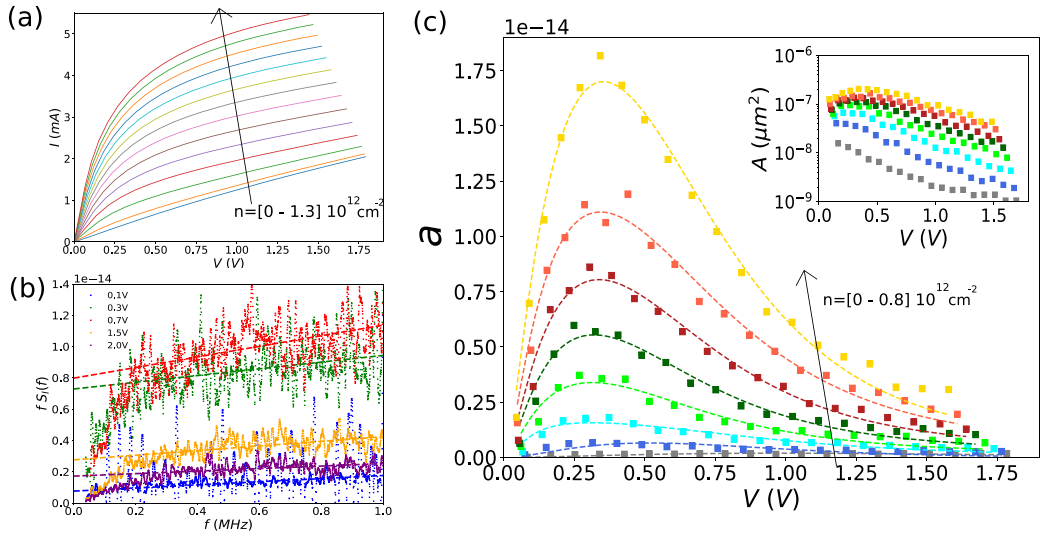

FIG. 1. DC transport and flicker noise in the high-mobility graphene transistor GRS5. (a) Current-voltage curves for doping $n = [0–1.3]10^{12}$ cm^{-2}. (b) Noise spectra in increasing bias at $n = 0.6\,10^{12}$ cm^{-2}. Dashed lines are linear fits of $fS_I(f) = a + bf$ of the data. Noise falls down below 0.2 MHz due to instrumental response. (c) Bell-shaped dependence of a versus V for $n = [0–0.8]10^{12}$ cm^{-2}; inset shows a semi-log plot of $A = fS_I/(GV)^2LW$ for same doping values indicating an exponential decay of A with bias.

III. HIGH-BIAS NOISE ANALYSIS

We start our analysis by focusing on the velocity saturation regime, which is exemplified in the sample "Lyon1" where the Zener contribution to transport is minimized to $\sigma_Z \simeq 0.1$ mS (Table SI-1), as deduced from the fitting of the differential conductance in Fig. 2(a) data. Consistently, noise thermometry [Fig. 2(a), inset] shows little fingerprint of Zener cooling, as opposed to other samples where a prominent breakout of the $T_N(E)$ dependence signals its ignition (see Supplementary Material Figs. SI-6). The origin of Zener transport suppression in "Lyon1" is discussed below. Importantly, the velocity flicker noise in Fig. 2(b) reduces to its velocity-saturation contribution $fS_{\rm sat}LW = Av^2 = A[\mu(E)E]^2$, which is entirely determined by the differential mobility $\mu(E)$:

$$fS_{\rm sat}LW = A\times v_{\rm sat}^2\left[\frac{E/E_{\rm sat}}{(1+E/E_{\rm sat})^2}\right]^2. \qquad (1)$$

It is characterized by a quadratic low-bias onset $fS_{\rm sat}LW = A[\mu(0)E]^2$, consistent with standard Hooge law $fS_ILW = A(I)^2$, a peak $fS_{\rm sat}LW = Av_{\rm sat}^2/16$ at $E = E_{\rm sat}$, and a high-bias tail $fS_{\rm sat}LW = Av_{\rm sat}^2(E_{\rm sat}/E)^2$. The orange and brown dashed lines in Fig. 2(b) are examples of theoretical fits with Eq. (1) for the $n = 0.7$ and $n = 1.1\ 10^{12}$ cm^{-2} data. The quasiscaling observed here (and in Figs. SI-5) relies on the weak doping dependence of $v_{\rm sat}$ [hence $E_{\rm sat} = v_{\rm sat}/\mu(0)$, $\mu(0)$ being doping independent]. From the $n = 7.10^{11}$ cm^{-2} data we deduce $A \simeq 6.4\ 10^{-7}$ μm^2, which is consistent with diffusive-graphene literature [16]. Setting $A = 2\alpha_0/\pi n_\Delta$ in an IR bremsstrahlung spirit, we infer $n_\Delta \simeq 0.7\ 10^{12}$ cm^{-2}.

We now turn to the more general case where a significant Zener contribution is observed at high field, in both the DC transport (Fig. SI-4) and in the noise thermometry (Fig. SI-6 and Fig. 3, insets). We rely on a two-fluid expression of current noise

$$fS_I(V)LW = (G_{\rm sat}V)^2A + (G_ZV)^2Be^{-V/V_\Lambda}, \qquad (2)$$

generalizing Eq. (1) by the inclusion of a Zener term of amplitude Be^{-V/V_Λ}. As conductance $G_Z(V) = $ Cst., the exponential high-bias drop-off factor, with a cutoff voltage V_Λ (and field E_Λ), is necessary to avoid a divergence of noise and match the experimental exponential decay in Fig. 1(c), inset. Note that the parameter A introduced here refers to the sole intraband noise, in opposition to the rough estimate of A in Fig. 1(c) that stems from the total noise: both definitions coincide in the low-bias extrapolate where interband noise is negligible. The noise fitting procedure is detailed in Supplementary Material Sec. I. In a first step we fit the $S_I(V)$ data with Eq. (2) using A, B, and V_Λ as independent parameters, where we find $A(n) \simeq Cst.$, $V_\Lambda(n) \simeq Cst.$ and $B(n) \propto n^2$. Combined to $G_{\rm sat} \propto n$, it suggests a doping-independent velocity noise $S_v(n) = S_I(n)/(neW)^2$.

Using the ansatz $A = 2\alpha_0/\pi n_\Delta$, where the density n_Δ is on the order of the out-of-equilibrium electron-hole pair density induced by Zener tunneling and hyperbolic cooling [27], we introduce a "Zener mobility" $\mu_Z = \sigma_Z/en_\Delta$ and a "Zener velocity" $v_Z = \mu_ZE_\Lambda$. Velocity noise rewrites

$$fS_vLW = A[\mu_{\rm sat}(E)E]^2 + B\frac{n_\Delta^2}{n^2}[\mu_ZE]^2e^{-E/E_\Lambda}, \qquad (3)$$

where $B\frac{n_\Delta^2}{n^2} \simeq Cst. \sim 100\,A$ over the sample series. We notice that $\frac{Bn_\Delta^2}{An^2} \sim \frac{\alpha_g}{\alpha_0} = 96$, where α_0 and $\alpha_g = e^2/4\pi\epsilon_0\epsilon_{hBN}\hbar v_F \simeq 0.70$ are the fine-structure constants of vacuum and hBN-encapsulated graphene, respectively (taking $\epsilon_{\rm hBN} = 3.4$ [33]). Consequently, we set for definiteness $\frac{Bn_\Delta^2}{An^2} = \frac{\pi\alpha_g}{2\alpha_0} = 150$ to rewrite velocity noise in a two-parameter two-fluid expression

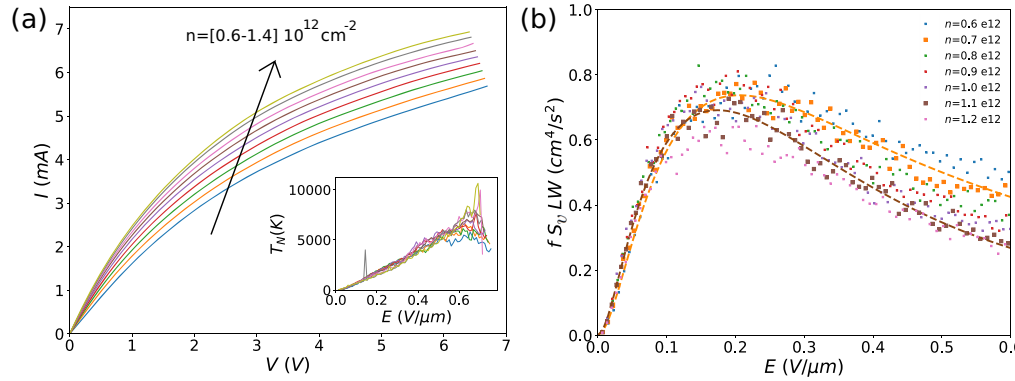

FIG. 2. DC transport and flicker noise in the graphene transistor "Lyon1." (a) Current-voltage and noise thermometry (inset) curves for doping $n = [0.6–1.4]10^{12}$ cm^{-2}, (b) Quasiscaling of the velocity flicker noise $fS_vLW(E)$ as a function of electric field $E = V/L$. The representative $n = 0.7\ 10^{12}$ cm^{-2} (or $n = 1.1\ 10^{12}$ cm^{-2}) data are well fitted by Eq. (1) with $A = 6.4\ 10^{-7}$ μm^2 and $v_{\rm sat} = 0.82\, v_F$ (or $A = 4.6\ 10^{-7}$ μm^2 and $v_{\rm sat} = 0.65\, v_F$).

$$S_v = S_{\rm sat} + S_{\rm Zener},$$

$$fS_vLW = Av_{\rm sat}^2\left[\frac{E/E_{\rm sat}}{(1+E/E_{\rm sat})^2}\right]^2 + \frac{\pi\alpha_g}{2\alpha_0}Av_Z^2\left[\frac{E}{E_\Lambda}e^{-E/2E_\Lambda}\right]^2. \tag{4}$$

The Zener contribution also has a bell-shaped bias dependence (brackets), with a E^2 low-bias dependence, a peak $fS_{\rm Zener}LW = 4\frac{\pi\alpha_g}{2\alpha_0}Av_Z^2/e^2$ at $E = 2E_\Lambda$, and an exponential tail. The two contributions have similar peak amplitudes for $v_{\rm sat}/v_Z \sim 8e^{-1}\sqrt{\frac{\pi\alpha_g}{2\alpha_0}} \simeq 36$, with peak positions shifted by a factor of 2 for $E_{\rm sat} \sim E_\Lambda$ in such a way that $S_{\rm Zener}$ prominently affects the high-field tail of the flicker noise, when $S_{\rm sat}$ accounts for the flicker noise onset.

Figure 3 compares velocity flicker noise data at the representative doping $n = 6.10^{11}$ cm^{-2} for six devices of the series. As seen in the figure, the bias dependencies generally deviate from the velocity-saturation bell shape of Fig. 2(b) described by Eq. (1). Figure 3 also shows fits (orange lines) with the two-fluid Eq. (4), using n_Δ and E_Λ as the only free parameters. The velocity-saturation (green lines) and Zener (red lines) components are displayed in each panel. A good agreement with the two-fluid model is observed with, however, some deviations at extremely high bias in few devices [see, e.g.,

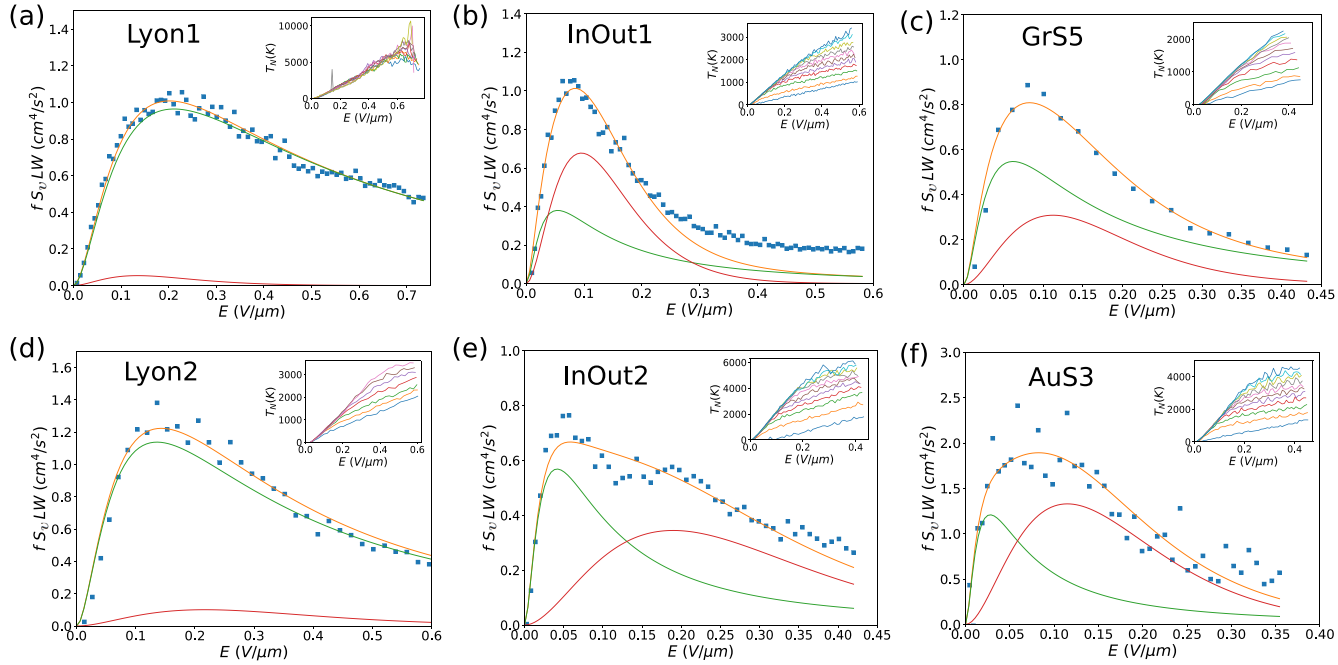

FIG. 3. Velocity flicker noise fS_vLW for six typical devices at a representative doping $n = 6\ 10^{11}$ cm^{-2} (dots), and their fits with Eqs. (1) and (4) for the two-fluid model. Green (red) lines correspond to the saturation (Zener) contribution, orange lines are their sum. Successive panels correspond to devices of increasing mobility $\mu = 4 \rightarrow 15\,\mathrm{m}^2/\mathrm{Vs}$ (Table SI-1). Insets show for each device the noise temperature T_N as function of bias and doping measured in the $f = [1–10]$ GHz range, as detailed in the Supplementary Material Fig. SI-6.

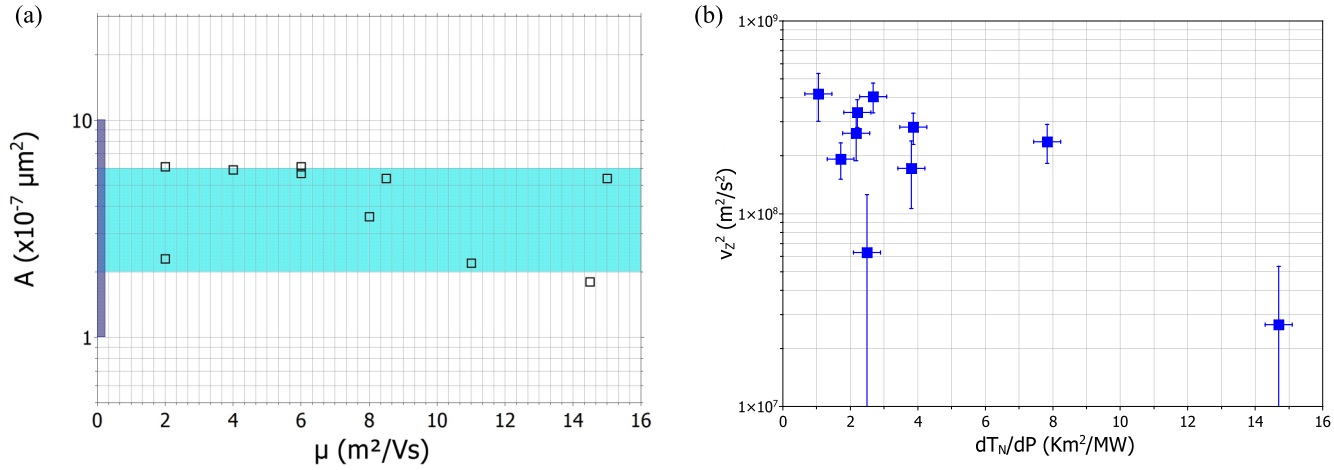

FIG. 4. Flicker-noise correlations to mobility and Zener cooling. (a) Noise amplitude A as function of mobility for ten devices of the series (dots). The light-blue rectangle corresponds to our hBN-encapsulated graphene devices and the dark-blue rectangle to literature data. (b) Zener-flicker amplitude v_Z^2 as function of the thermal resistance dT_N/dP to the hBN substrate in the Zener interband regime.

Fig. 3(b), with a high-bias noise tail at a nonzero value due to an unknown additional spurious mechanism. The Zener contribution is tiny in the "Lyon1" device [Fig. 3(a)], justifying the analysis of Fig. 2(b) in terms of the only saturation contribution. A similar trend is observed in "Lyon2" [Fig. 3(d)], which is made with the same PDC-grade hBN [32]. Other devices, fabricated with HPHT-grade hBN [31], exhibit more prominent cooling in the Zener regime (see Fig. 3, insets). In these devices, single-fluid fits are unable to map the observed field dependencies, justifying our "two-fluid" analysis (further confirmed by the comparable amplitudes of the two contributions). As expected, the saturation contribution is mostly responsible for the onset of flicker noise at low bias. The Zener contribution becomes significant at larger bias, with a peak at $2E_\Lambda > E_{\rm sat}$, explaining the slower decrease of flicker noise at high bias.

IV. TWO-FLUID INTERPRETATION

We now discuss the sample-dependent parameters A (or n_Δ) and E_Λ, which are listed in Table SI1. We obtain $A \in [2\text{–}7]\,10^{-7}$ µm^2 [light-blue domain in Fig. 4(a)], corresponding to $n_\Delta \in [0.7\text{–}2.3]\,10^{12}$ cm^{-2}. These values, obtained in a broad $\mu(0) \in [2\text{–}15]$ m^2/Vs mobility range, confirm the literature data $A \in [10^{-7}\text{–}10^{-6}]$ µm^2 for diffusive SiO_2-supported graphene, suggesting that A is essentially impurity-scattering insensitive. The similarity of flicker noise amplitude A in the impurity-dominated (linear low-mobility) and OP-dominated (nonlinear high-mobility) scattering regimes, reflects its universal character. The characteristic field for the Zener term $E_\Lambda = 75 \pm 25$ mV/µm is quite similar along the device series. It can be converted into a Zener junction length $\Lambda = \sqrt{\hbar v_F/eE_\Lambda} = 100 \pm 15$ nm, which shows a reduced dispersion compared to the quite spread values of the Zener conductivity $\sigma_Z \in [0.1\text{–}1]$ mS.

The light-blue n_Δ domain in Fig. 4(a) can be expressed in terms of an energy range $\tilde{\Delta} = \hbar v_F \sqrt{\pi n_\Delta}$ relying on the massless dispersion of graphene. In doing so we find that $\tilde{\Delta} \in [\Delta_1, \Delta_2] = [0.09\text{–}0.17]$ eV is actually bounded by the lower and upper RS bands of hBN. These two energies being associated [27] to momentum and energy relaxations, respectively, it suggests that flicker noise in high-mobility graphene maps the ambivalent nature of conductance as an admixture of momentum and energy relaxations parameters.

Flicker noise correlation to energy relaxation is even more obvious in the Zener contribution, which is characterized by a large amplitude and the characteristic velocity $v_Z = \sigma_Z E_\Lambda / e n_\Delta$ in Eq. (4). The semi-log plot $v_Z^2(dT_N/dP)$ in Fig. 4(b) indeed shows a strong decrease of the Zener flicker amplitude with the thermal resistance to the hBN substrate, confirming the trend observed on sample "Lyon1." The reduced Zener cooling in the two "Lyon" devices is attributed to the larger hBN structural disorder obtained through the PDC route. The hBN structural quality is indeed essential to ensure free propagation of hyperbolic phonon polaritons (HPhP) in the hBN bulk; their strong backscattering/damping in PDC-hBN devices is likely to suppress the MIR electromagnetic coupling, implying lower Zener conductivity and radiative cooling, resulting in a smaller Zener flicker noise.

We now interpret the Zener term in Eq. (4). It is characterized by a large coupling constant $\alpha_g \sim 100\times\alpha_0$ that is affected by a field reduction factor e^{-E/E_Λ} with a nearly sample-independent characteristic field $E_\Lambda \simeq 75$ mV/µm. We can convert it to an energy scale $\varepsilon_\Lambda = \sqrt{e\hbar v_F E_\Lambda} = 7$ meV, and length $\Lambda = \hbar v_F/\varepsilon_\Lambda = 100$ nm of Zener tunneling. In this interpretation, ε_Λ and Λ are the characteristic energy and length of coherent tunneling, which are limited by inelastic HPhP scattering. They control the Hooge parameter $\alpha_g e^{-E/E_\Lambda}$ in a quantum-coherent bremsstrahlung interpretation [13]. Besides, note that the quantum-incoherent theory of flicker noise involves a reduction factor $v_F^2/c^2 \ll 1$ (c the speed of light) with respect to the coherent one $\alpha_H = 2\alpha_0/\pi$ [13]. Further insight requires a comprehensive theoretical approach, including geometrical antenna effects in free-light and HPhP emissions, which is beyond the scope of this experimental report.

V. CONCLUSION

The conclusion of our experimental report of α-noise in hBN-encapsulated graphene is twofold. First, we generalize the Hooge formula for nonlinear intraband transport by substituting the total current I with the differential current GV. We give an interpretation of the graphene constant flicker noise prefactor in terms of a scattering density n_Δ, defined by an effective energy $\tilde{\Delta}$ interpolating between the elastic-scattering Δ_1 and the inelastic-scattering Δ_2 energies. Second, we extend the Hooge formula to include the Zener transport contribution at high field. We propose a compact formula, in the spirit of the bremsstrahlung interpretation of flicker noise, with a strongly enhanced interband amplitude reflecting the large coupling of graphene electron-hole pairs to near-field HPhPs of hBN [29]. The graphene case corresponds to the collective strongly inelastic variant, where IR bremsstrahlung constitutes the main energy-relaxation mechanism in the Zener regime with $\alpha_H \sim \alpha_g \sim 1$. The superposition of the two terms in the two-fluid α-noise analysis accounts for the observed field dependencies in a series of graphene transistors with varied IR environments. Experiment indicates that the interband coupling constant is affected by an exponential suppression factor accounting for decoherence effects in the HPhP coupling. Our observations that (i) intraband Hooge parameter approaches the Handel limit $\alpha_{H,\mathrm{intra}} = 2\alpha_0/\pi$, (ii) interband parameter is strongly enhanced by a factor of 100, (iii) is sensitive to decoherence effects via the $\exp(-E/E_\Lambda)$ factor, and (iv) and the correlation of flicker noise with thermal conductance to the hBN substrate, constitute four qualitative indications supporting the quantum-coherent bremsstrahlung interpretation of flicker noise. In addition, this interpretation naturally explains the ubiquitous scatter in flicker data by the variability in the IR environment. In a broader perspective, our work promotes flicker noise, in complement to DC transport and noise thermometry, as a powerful semi-quantitative tool to decipher the physical mechanisms at stake in graphene transistors under extreme bias. Flicker noise is also important for modern quantum technologies, as $1/f$ noise is considered as an important source of decoherence [36].

Data are available on a Zenodo repository at Ref. [37].

ACKNOWLEDGMENTS

The authors thank Gerbold Ménard for his critical reading of the manuscript. The research leading to these results received partial funding from the European Union Horizon 2020 research and innovation program under Grant Agreement No. 881603 "Graphene Core 3," and from the French Grant No. ANR-21-CE24-0025-01 "ELuSeM."

[1] J. Clarke and G. Hawkins, Phys. Rev. B **14**, 2826 (1976).
[2] M. Kobayashi and T. Musha, IEEE Trans. Biomedic. Engin. **BME-29**, 456 (1982).
[3] R. T. Baillie, J. Business Eco. Stat. **16**, 273 (1998).
[4] P. Robin, M. Lizée, Q. Yang, T. Emmerich, A. Siria, and L. Bocquet, arXiv:2302.04468.
[5] A. L. McWorther, *Semiconductor Surface Physics*, edited by R. H. Kingston (University of Pennsylvania Press, Philadelphia, 1957), pp. 207–228.
[6] M. A. Caloyannides, J. Appl. Phys. **45**, 307 (1974).
[7] P. Dutta and P. M. Horn, Rev. Mod. Phys. **53**, 497 (1981).
[8] F. N. Hooge, Phys. Lett. A **29**, 139 (1969).
[9] F. N. Hooge and A. M. H. Hoppenbrouwers, Physica **45**, 386 (1969).
[10] F. N. Hooge, T. G. M. Kleinpenning, and L. K. J. Vandamme, Rep. Prog. Phys. **44**, 479 (1981).
[11] Sh. Kogan, *Electronic Noise and Fluctuations in Solids* (Cambridge University Press, Cambridge, England, 1996).
[12] P. H. Handel, Phys. Rev. Lett. **34**, 1492 (1975).
[13] P. H. Handel, Phys. Stat. Sol. (b) **194**, 393 (1996).
[14] T. M. Nieuwenhuizen, D. Frenkel, and N. G. van Kampen, Phys. Rev. A **35**, 2750 (1987).
[15] M. B. Weissman, Rev. Mod. Phys. **60**, 537 (1988).
[16] A. A. Balandin, Nat. Nanotechnol. **8**, 549 (2013).
[17] N. Mavredakis, W. Wei, E. Pallecchi, D. Vignaud, H. Happy, R. Garcia Cortadella, A. Bonaccini Calia, J. A. Garrido, and D. Jiménez, ACS Appl. Electron. Mater. **1**, 2626 (2019).
[18] Y. M. Lin and P. Avouris, Nano Lett. **8**, 2119 (2008).
[19] S. Rumyantsev, G. Liu, W. Stillman, M. Shur, and A. A. Balandin, J. Phys.: Condens. Matter **22**, 395302 (2010).
[20] S. Takeshita, S. Matsuo, T. Tanaka, S. Nakaharai, K. Tsukagoshi, T. Moriyama, T. Ono, T. Arakawa, and K. Kobayashi, Appl. Phys. Lett. **108**, 103106 (2016).
[21] A. Rehman, J. A. Delgado Notario, J. Salvador Sanchez, Y. M. Meziani, G. Cywinski, W. Knap, A. A. Balandin, M. Levinshtein, and S. Rumyantsev, Nanoscale **14**, 7242 (2022).
[22] C. C. Kalmbach, F. J. Ahlers, J. Schurr, A. Muller, J. Feilhauer, M. Kruskopf, K. Pierz, F. Hohls, and R. J. Haug, Phys. Rev. B **94**, 205430 (2016).
[23] M. Kumar, A. Laitinen, D. Cox, and P. J. Hakonen, Appl. Phys. Lett. **106**, 263505 (2015).
[24] C. R. Dean, A. F. Young, I. Meric, C. Lee, L. Wang, S. Sorgenfrei, K. Watanabe, T. Taniguchi, P. Kim, K. L. Shepard, and J. Hone, Nat. Nanotech. **5**, 722 (2010).
[25] S. Dai, Q. Ma, M. K. Liu, T. Andersen, Z. Fei, M. D. Goldflam, M. Wagner, K. Watanabe, T. Taniguchi, M. Thiemens, F. Keilmann, G. C. A. M. Janssen, S.-E. Zhu, P. Jarillo-Herrero, M. M. Fogler, and D. N. Basov, Nat. Nanotech. **10**, 682 (2015).
[26] A. Kumar, T. Low, K. H. Fung, P. Avouris, and N. X. Fang, Nano Lett. **15**, 3172 (2015).
[27] W. Yang, S. Berthou, X. Lu, Q. Wilmart, A. Denis, M. Rosticher, T. Taniguchi, K. Watanabe, G. Fève, J. M. Berroir, G. Zhang, C. Voisin, E. Baudin, and B. Plaçais, Nat. Nanotechnol. **13**, 47 (2018).
[28] K-J. Tielrooij, N. C. H. Hesp, A. Principi, M. B. Lundeberg, E. A. A. Pogna, L. Banszerus, Z. Mics, M. Massicotte, P. Schmidt, D. Davydovskaya, D. G. Purdie, I. Goykhman, G. Soavi, A. Lombardo, K. Watanabe, T. Taniguchi, M. Bonn, D. Turchinovich, C. Stampfer, A. C. Ferrari *et al.*, Nat. Nanotechnol. **13**, 41 (2018).

[29] E. Baudin, C. Voisin, and B. Plaçais, Adv. Funct. Mater. **30**, 1904783 (2020).

[30] See Supplemental Material at http://link.aps.org/supplemental/10.1103/PhysRevB.107.L161104 for a summary of the geometrical and electronic properties of the transistors series, as well as a description of the measurement setup. It also contains further information about the two-fluid analysis described below and additional figures.

[31] T. Taniguchi and K. Watanabe, J. Crystal Growth **303**, 525 (2007).

[32] C. Maestre, Y. Li, V. Garnier, P. Steyer, S. Roux, A. Plaud, A. Loiseau, J. Barjon, L. Ren, C. Robert, B. Han, X. Marie, C. Journet, and B. Toury, 2D Mater. **9**, 035008 (2022).

[33] A. Pierret, D. Mele, H. Graef, J. Palomo, T. Taniguchi, K. Watanabe, Y. Li, B. Toury, C. Journet, P. Steyer, V. Garnier, A. Loiseau, J-M. Berroir, E. Bocquillon, G. Fève, C. Voisin, E. Baudin, M. Rosticher, and B. Plaçais, Mater. Res. Express **9**, 065901 (2022).

[34] A. Schmitt, P. Vallet, D. Mele, M. Rosticher, T. Taniguchi, K. Watanabe, E. Bocquillon, G. Fève, J. M. Berroir, C. Voisin, J. Cayssol, M. O. Goerbig, J. Troost, E. Baudin, and B. Plaçais, Nat. Phys. Online (2023).

[35] I. Meric, M. Y. Han, A. F. Young, B. Ozyilmaz, P. Kim, and K. L. Shepard, Nat. Nanotechnol. **3**, 654 (2008).

[36] E. Paladino, L. Faoro, G. Falci, and R. Fazio, Phys. Rev. Lett. **88**, 228304 (2002).

[37] https://doi.org/10.5281/zenodo.7632159.